Porous Mesostructured Zirconium Oxophosphate with Cubic ($Ia\bar{3}d$) Symmetry

Freddy Kleitz,[†] Stuart J. Thomson,[†,‡] Zheng Liu,[§] Osamu Terasaki,[§] and and Ferdi Schüth*[,†]

Max-Planck-Institut für Kohlenforschung, 45470 Mülheim an der Ruhr, Germany, and Japan Science and Technology Corporation (CREST) and Department of Physics, Tohoku University, Sendai 980-8578, Japan

Received February 1, 2002. Revised Manuscript Received August 8, 2002

We report the synthesis and characterization of a mesoporous zirconium oxophosphate with a cubic $Ia\bar{3}d$ symmetry. The ordered porous material was obtained by supramolecular self-assembly of a specific cationic surfactant combined with zirconium sulfate as inorganic precursor. A systematic investigation of the effects of initial reagent ratios and synthesis procedures is reported. Both the as-prepared and the template-free cubic porous zirconium oxophosphate materials were characterized by X-ray diffraction and transmission electron microscopy. The template-free material was additionally characterized by N_2 sorption. The removal of the template was studied by thermogravimetry/differential thermal analysis coupled with mass spectrometry and in situ high-temperature XRD. In addition, pyridine sorption-FTIR experiments were performed to evaluate the Lewis and Brønsted acidity.

Introduction

The growing interest in new porous materials with large surface areas, well-defined structures, and large pores has led to the discovery of numerous ordered mesoporous materials with special chemical and physical properties. A large number of materials with diverse mesoscopic structures and varying compositions have been reported and reviewed recently.[1−4] In contrast to silica-based mesoporous materials,[5−7] nonsiliceous ordered mesoporous materials have attracted considerably less attention, due to the relative difficulty in applying the same synthesis principles to non-silicate species. Nonsiliceous frameworks are usually more susceptible to redox reactions, hydrolysis, or phase transformations. Furthermore, these materials are generally less thermally stable, and many collapse totally upon removal of the template molecules.[8,9] However, the potential diversity of chemical, electrical, magnetic, and optical properties that can be envisaged makes transition metal-based ordered mesoporous materials extremely attractive.[10,11] Therefore, transition metal-based ordered mesoporous materials have been synthesized based on titanium,[12−15] zirconium,[15−17] niobium,[18] or tantalum,[19] most of them being either hexagonally ordered or rather disordered. However, less attention has been given to nonhexagonal structures, due mainly to the higher difficulty in achieving stable well-ordered porous solids. Neeray and Rao[20] described a cubic $Ia\bar{3}d$ zirconium-based mesophase obtained by a phase transformation. However, the possibility of removal of the template was not discussed in this case. Antonelli et al.[21] showed that it is also possible to form 3-D hexagonal ($P6_3mmc$) and cubic ($Pm3n$) niobium oxide-based mesophases; but removal of the template was not successful. Furthermore, Hatayama et al.[22] reported the synthesis of a well-ordered mesostructured cubic $Ia\bar{3}d$ vanadium phosphorus oxide, which was, however, again not stable upon template removal. To our knowledge, the cubic

* To whom correspondence should be addressed. E-mail: schueth@mpi-muelheim.mpg.de.
† Max-Planck-Institut für Kohlenforschung.
‡ Present address: Materials Division, Building 3, ANSTO, PMB 1, Menai, 2234, New South Wales, Australia.
§ Tohoku University.

(1) Ciesla, U.; Schüth, F. *Microporous Mesoporous Mater.* **1999**, *27*, 131.
(2) Lindén, M.; Schacht, S.; Schüth, F.; Steel, A.; Unger, K. K. *J. Porous Mater.* **1998**, *5*, 177.
(3) Ying, J. Y.; Mehnert, C. P.; Wong, M. S. *Angew. Chem., Int. Ed.* **1999**, *38*, 56.
(4) Corma, A. *Chem. Rev.* **1997**, *97*, 2373.
(5) Beck, J. S.; Vartuli, J. C.; Roth, W. J.; Leonowicz, M. E.; Kresge, C. T.; Schmitt, K. D.; Chu, C. T.-W.; Olson, D. H.; Sheppard, E. W.; McCullen, S. B.; Higgins, J. B.; Schlenker, J. L. *J. Am. Chem. Soc.* **1992**, *114*, 10834.
(6) Yanagisawa, T.; Shimizu, T.; Kuroda, K.; Kato, C. *Bull. Chem. Soc. Jpn.* **1990**, *63*, 988.
(7) Zhao, D.; Feng, J.; Huo, Q.; Melosh, N.; Fredrickson, G. H.; Chmelka B. F.; Stucky, G. D. *Science* **1998**, *279*, 548.
(8) Ciesla, U.; Demuth, D.; Leon, R.; Petroff, P.; Stucky, G. D.; Unger, K.; Schüth, F. *J. Chem. Soc., Chem. Commun.* **1994**, 1387.
(9) Zhao, D.; Goldfarb, D. *Chem. Mater.* **1996**, *8*, 2571.
(10) Sayari, A. *Chem. Mater.* **1996**, *8*, 1840.
(11) Schüth, F. *Chem. Mater.* **2001**, *13*, 3184.
(12) Antonelli, D. M.; Ying, J. Y. *Angew. Chem., Int. Ed. Engl.* **1995**, *34*, 2014.
(13) Blanchard, J.; Trens, P.; Hudson, M.; Schüth, F. *Microporous Mesoporous Mater.* **2000**, *39*, 163.
(14) Bhaumik, A.; Inagaki, S. *J. Am. Chem. Soc.* **2001**, *123*, 691.
(15) Yang, P.; Zhao, D.; Margolese, D. I.; Chmelka, B. F.; Stucky, G. D. *Chem. Mater.* **1999**, *11*, 2813.
(16) Ciesla, U.; Schacht, S.; Stucky, G. D.; Unger, K.; Schüth, F. *Angew. Chem., Int. Ed. Engl.* **1996**, *35*, 541.
(17) Wong, M. S.; Ying, J. Y. *Chem. Mater.* **1998**, *10*, 2067.
(18) Antonelli, D. M.; Ying, J. Y. *Angew. Chem., Int. Ed. Engl.* **1996**, *35*, 426.
(19) Antonelli, D. M.; Ying, J. Y.*Chem. Mater.* **1996**, *8*, 874.
(20) Neeray, S.; Rao, C. N. R. *J. Mater. Chem.* **1998**, *8*, 1631.
(21) Antonelli, D. M.; Nakahira, A.; Ying, J. Y. *Inorg. Chem.* **1996**, *35*, 3126.
(22) Hatamaya, H.; Misono, M.; Taguchi, A.; Mizuno, N. *Chem. Lett.* **2000**, 884.

10.1021/cm021128d CCC: $22.00
Published on Web 09/21/2002

*Im*3*n* mesoporous TiO_2 described by Stucky and coworkers in 1998 remains until now the only template-free 3-D mesophase reported.[15,23]

Well-ordered 3-D porous networks with large pores and high surface areas can present very attractive features as supports or hosts for active species, flow and transport technologies, in delivery and release, separation techniques, and catalysis. Especially for diffusion of reactants within the structure, a 3-D channel structure is expected to have advantages over a 2-D orientated hexagonal one.[24−30]

We reported previously the synthesis of zirconium oxophosphate mesoporous materials,[16,31] The ZrO_xP_y meso-structured materials were obtained by the self-assembly of a zirconium sulfate−alkylammonium mesophase that was subsequently modified by treatment with phosphoric acid. The material exhibits a well-ordered hexagonal structure, and with the substitution of sulfate by phosphate, a thermally stable porous solid results. Zirconium-based materials are commonly used as industrial catalysts or supports. Therefore, well-ordered zirconium oxophosphate materials, showing relatively large adsorption capacity, high surface area with Lewis and Brønsted acidity, may be suitable for acid-catalyzed reactions.[32] The desire to create porous materials combining such acid−base properties and the advantages of a well-defined 3-D structure led us to the synthesis of a cubic $Ia\bar{3}d$ mesoporous zirconium-based analogue.[33] However, in these initial studies, we were unable to remove the template without structural collapse.

By carefully examining the synthesis conditions and the removal of the template, which was highly unclear, we succeeded in removing the template without destroying the structure.[34] We now report in detail on the first cubic $Ia\bar{3}d$ nonsiliceous porous material. Its synthesis was based on a zirconium oxophosphate mesophase with the use of a simple cationic surfactant. We describe details of the synthesis and the effects on the properties of the material upon varying the composition of the initial mixture. The question of template removal is addressed and investigated by TG-DTA coupled with mass spectrometry and in situ XRD. The porous materials are characterized by XRD, high-resolution transmission electron microscopy, and N_2 sorption. Furthermore, the acidity of the materials is evaluated by pyridine sorption-FTIR.

Experimental Section

Reagents. *N*-Benzyl-*N*,*N*-dimethyloctadecylammonium chloride hydrate (*N*-benzyl-*N*,*N*-dimethylstearylammonium chloride hydrate; C18BDAC, purity 90%, Aldrich) was used as the structure-directing agent. $Zr(SO_4)_2 \cdot 4H_2O$ purchased from Alfa was used as the zirconium source. Postsynthetic treatments were performed with a solution of orthophosphoric acid (Fluka 85%). All chemicals were used as received.

Synthesis. The synthesis was derived from the method described by Ciesla **e**t al.[16,31] The reactant molar ratio was $Zr(SO_4)_2$:C18BDAC:H_2O = 1/0.27−0.80/477. In a typical synthesis, 3.04 g (6.87 mmol) of surfactant was dissolved in 85 g of distilled water at 35 °C. To this mixture, a solution of 4.55 g of zirconium sulfate (12.8 mmol) dissolved in 25 g of H_2O was added at once. A precipitate formed instantaneously, and the mixture was left under stirring for 2 h. The mixture was transferred to a polypropylene bottle and stored for 3 days at 90 °C, under static conditions. After cooling, the mixture was filtered and rinsed with 50 mL of distilled water. The solid collected was then added to an aqueous solution of 100 mL of H_3PO_4 (0.5 M) and stirred for 4−5 h at room temperature. The resultant product was filtered, washed with 100 mL of distilled water, and dried overnight in air at 90 °C. Samples were isolated at intermediate stages during the synthesis procedure. Additionally, the synthesis batches were scaled up by a factor of 3 for selected surfactant-to-zirconium sulfate ratios for testing purposes; these samples are denoted (B).

Template-free products were obtained after calcination in a box furnace in air for 5 h at either 500 °C or 550 °C, or for 3 h at 300 °C followed by 3 h at 500 °C.

Characterization Methods. The X-ray diffraction measurements were performed on a Stoe STADI P transmission X-ray powder diffractometer, using Cu−Kα1 radiation and equipped with a linear position-sensitive detector. XRD patterns were recorded in the ranges of 1−10° (2θ) with a step of 0.5° (2θ), time/step of 60 or 120 s, and in the ranges of 8−32° (2θ) with a step of 0.5 ° (2θ), and time/step of 60 s.

The high-temperature XRD measurements were recorded on a Stoe STADI P $\theta-\theta$ reflection powder X-ray diffractometer using Cu−Kα1+2 radiation with secondary monochromator and scintillation detector. Details of the experimental procedure have been described elsewhere.[35] A high-temperature X-ray diffraction chamber (Johanna Otto HDK S1), with a Pt/Rh heating element as a sample holder was used. XRD patterns were recorded with automatic divergence slit (receiving slit fixed at 0.8 mm) in a range of 1.2−6° (2θ) with a step of 0.05° (2θ) and time/step of 8 s.

For TEM observation, all samples were first dispersed in ethanol (99.9 vol %) using the ultrasonic method, and the suspension was subsequently dropped onto a carbon microgrid. High-resolution electron microscopy (HREM) observations were performed with a 400-kV electron microscope (JEM-4000EX). EDX was used for elemental analysis.

The thermogravimetric analyses combined with differential thermal analyses were performed on a Netzsch STA 449 C thermobalance coupled with a Balzers Thermostar 442 mass spectrometer. The measurements were carried out under air with a heating rate of 5 K/min in all the cases.

The N_2 sorption measurements were performed on a ASAP 2010 (Micromeritics) at liquid nitrogen temperature. Prior to the measurement, the calcined samples were activated under vacuum during 12 h at 200 °C. Some selected samples were also analyzed by argon adsorption at liquid argon temperature in a Sorptomatic 1900 (Carlo Erba). Textural parameters

(23) Yang, P.; Zhao, D.; Margolese, D. I.; Chmelka, B. F.; Stucky, G. D. *Nature* **1998**, *396*, 152.
(24) Zhang, W. Z.; Pinnavaia, T. J. *Catal. Lett.* **1996**, *38*, 261.
(25) Zhang, S. G.; Fujii, Y.; Yamashita, H.; Koyano, K.; Tatsumi, T.; Anpo, M. *Chem. Lett.* **1997**, *7*, 659.
(26) Chang, Z.; Krishna, R. M.; Xu, J.; Koodali, R.; Kevan, L. *Phys. Chem. Chem. Phys.* **2001**, *3*, 1699.
(27) Ryoo, R.; Jun, S.; Kim J. M.; Kim, M. J. *J. Chem. Soc., Chem. Commun*. **1997**, 2225.
(28) Walker, J. V.; Morey, M.; Carlsson, A.; Davidson, A.; Stucky, G. D.; Butler, A. *J. Am. Chem. Soc.* **1997**, *119*, 6921.
(29) Dai, L.-X.; Teng, Y.-H.; Tabata, K.; Suzuki, E.; Tatsumi, T. *Microporous Mesoporous* Mater. **2001**, *44*−*45*, 573.
(30) Hunter, H. M. A.; Wright, P. A. *Microporous Mesoporous Mater.* **2001**, *43*, 361.
(31) Ciesla, U.; Fröba, M.; Stucky, G. D.; Schüth, F. *Chem. Mater.* **1999**, *11*, 227.
(32) (a) Tanabe, K.; Yamagushi, T. *Catal. Today* **1994**, *20*, 185. (b) Yamagushi, T. *Catal. Today* **1994**, *20*, 199. (c) Huang, Y.-Y.; McCarthy, T. J.; Sachtler, W. M. H. *Appl. Catal. A: Gen.* **1996**, *148*, 135. (d) Clark, J. H.; Monks, G. L.; Nightingale, D. J.; Price, P. M.; White, J. F. *J. Catal.* **2000**, *193*, 348. (e) Guerrero-Ruiz, A.; Rodriguez-ramos, I.; Fierro, J. L. G.; Jimenez López, A.; Olivera Pastor, P.; Maireless Torres, P. *Appl. Catal. A: Gen.* **1992**, *92*, 81. (f) Xiao, J.; Xu, J.; Wu, Y.; Gao, Z. *Appl. Catal. A: Gen.* **1999**, *181*, 313.
(33) Schüth, F.; Ciesla, U.; Schacht, S.; Thieme, M.; Huo, Q.; Stucky, G. D. *Mater. Res. Bull.* **1999**, *34*, 483.
(34) Schüth, F. *Stud. Surf. Sci. Catal.* **2001**, *135*, 1.
(35) Kleitz, F.; Schmidt, W.; Schüth, F. *Microporous Mesoporous Mater.* **2001**, *44*−*45*, 95.

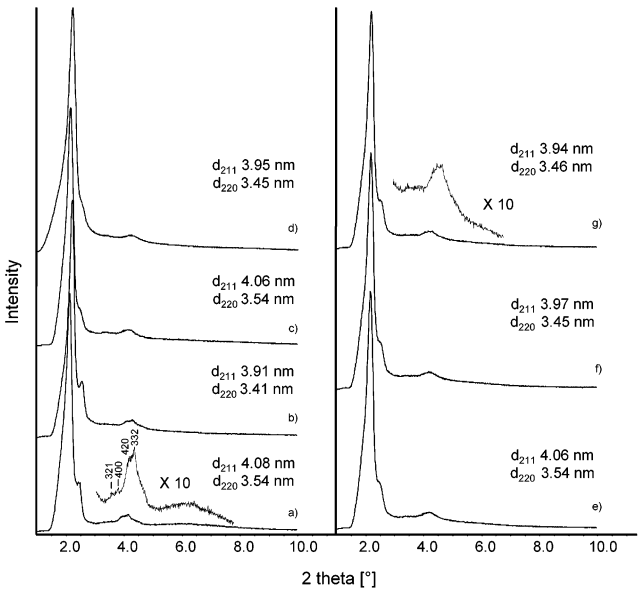

Figure 1. XRD patterns recorded for cubic zirconium oxide-based mesophases at different synthesis stages: (a) wet after 2 h of synthesis; (b) after a following drying period at 90 °C; (c) wet after aging 3 days at 90 °C; (d) after aging 3 days at 90 °C, dried at 90 °C; (e) wet zirconium oxophosphate obtained after phosphatation; (f) zirconium oxophosphate dried at room temperature; (g) zirconium oxophosphate dried at 90 °C overnight.

obtained with argon agreed well with those from nitrogen adsorption.

IR spectra of adsorbed pyridine were collected on a Nicolet 560 spectrometer equipped with a MCT detector. Samples were pressed from powder (using the same weight of powder for each corresponding to 10 mg/cm^2) and used as circular pressed pellets 25 mm in diameter. An in situ cell allowed evacuation ($\sim 3 \times 10^{-6}$ mbar), heating, and introduction of pyridine vapor to the sample. Each sample was heated to 200 °C for 12 h under vacuum to remove adsorbed water prior to the adsorption of pyridine. The sample was cooled to 140 °C, and spectra of the unexposed sample pellet were taken. For acidity measurements, the sample was exposed to 4 mbar of pyridine vapor at 140 °C and then evacuated.

Results

As-Synthesized Cubic Mesophase Based on Zirconium Oxide. Addition of the aqueous solution of zirconium sulfate to the surfactant solution leads to rapid formation of a zirconium sulfate−surfactant composite mesophase. The mesostructured material obtained under acidic condition is then hydrothermally aged and subsequently posttreated with an aqueous solution of phosphoric acid, following the method described previously.[16,31]

The XRD patterns presented in Figure 1 show the reflections corresponding to the bicontinuous cubic $Ia\bar{3}d$ material. The diffractograms were recorded after the synthesis mixture was stirred for 2 h, with subsequent measurements performed periodically at different synthesis stages. A pure cubic phase was obtained rapidly at room temperature and no intermediate phase was detected in the time range investigated (Figure 1).

The X-ray diffraction pattern recorded for a wet sample before hydrothermal treatment shows six reflections that can be indexed clearly to a $Ia\bar{3}d$ phase (Figure 1a). Compared to a silica-based cubic mesophase, the reflections appearing at ~4° (2θ) are only poorly resolved. Due to the low signal-to-noise ratio, no further attempts to index the higher (2θ) reflections were made. However, the analogy to the silica-based bicontinuous cubic MCM-48 mesophase[36] suggests that the material is cubic with a space group $Ia\bar{3}d$. For hydrothermally treated and phosphated samples, the d(211) and d(220) remain constant for the wet samples and dried ones, respectively. Upon drying, shrinkage of ~0.15 nm is observed in all cases (Figure 1). The unit cell parameter measured from the (211) line of the uncalcined dried material is generally $a_0 = \sim 9.85$ nm for as-synthesized materials. Only reflections within 2−8 ° (2θ), which are due to the ordering of the pores, are observed. This indicates that no condensed crystalline phases are present.

The hydrothermal treatment was carried out at 90 °C for 3 days to achieve a material that is expected to be thermally and mechanically much more stable. Although an improvement of the long-range ordering upon aging at 90 °C had been reported for the hexagonal zirconium sulfate equivalent mesophase,[37] the thermal aging results in the case of the cubic mesophase in a decrease of the higher order reflections resolution (Figure 1c). No variation in d spacing or phase transition could be observed. Our previous studies showed that the zirconium sulfate−surfactant composite mesophase is not thermally stable and that template removal by calcination leads to structural collapse. We described an efficient stabilizing method based on a postsynthetic treatment with phosphoric acid which replaces the sulfate groups by more thermally stable phosphate groups within the framework.[31] After cooling and filtering, the sample is treated with an aqueous solution of phosphoric acid. The $Ia\bar{3}d$ cubic mesophase phase is retained after phosphatation as shown in Figure 1e. However, a slightly less well-resolved XRD pattern finally results after drying (Figure 1g).

To study surfactant effects, the initial surfactant-to-zirconium sulfate molar ratio (r) was varied from 0.81 to 0.27. An observable trend is that samples with higher surfactant-to-zirconium ratio exhibit a cubic structure with better resolved XRD reflections (see representative examples in Figure 2a). This might suggest that higher initial amounts of surfactant used leads to better structural order. However, differences in wall thicknesses, size of the scattering domains, or variations in surface roughness could also explain the different resolutions.[38] The XRD results obtained on the as-synthesized mesophases are listed in Table 1. No significant variations in d spacing were observed with d(211) of ~4 nm. The sample synthesized with $r = 0.27$ exhibits a less well-resolved XRD pattern that cannot be clearly indexed as cubic $Ia\bar{3}d$ (not shown). In comparison, a sample synthesized with $r = 0.40$ without the hydrothermal aging period at 90 °C shows a substantially larger d spacing value (4.22 nm). However, the XRD pattern of this sample indicates a rather disor-

(36) Monnier, A.; Schüth, F.; Huo, Q. S.; Kumar, D.; Margolese, D. I.; Maxwell, R. S.; Stucky, G. D.; Krishnamurty, M.; Petroff, P.; Firouzi, A.; Janicke, M.; F. Chmelka, B. F. *Science* **1993**, *261*, 1299.

(37) Lindén, M.; Blanchard, J.; Schacht, S.; Schunk, S.; Schüth, F. *Chem. Mater.* **1999**, *11*, 3002.

(38) Sauer, J.; Marlow, F.; Schüth, F. *Phys. Chem. Chem. Phys.* **2001**, *3*, 1.

Table 1. Structural and Adsorption Properties of Cubic Zirconium Oxophosphate Synthesized with Different Surfactant-to-Zirconium Ratios[a]

r	*d*(211) as made (nm)	*d*(211) calcined (nm)	a_0 calcined (nm)	total vol adsorbed (cm^3/g)	surface area eq BET[b] (m^2/g)	pore volume[c] (cm^3/g)
0.80	4.00	2.48	6.07	21	64	0.03
0.67	4.02	2.59	6.34	47	149	0.07
0.67 (B)	4.01	2.55	6.27	19	56	0.03
0.67 (B) plateau[d]	4.01	2.58	6.32	52	164	0.08
0.59	4.02	2.66	6.52	55	173	0.08
0.54	3.95	2.72	6.66	54	168	0.08
0.54 plateau[d]	3.95	2.76	6.76	79	251	0.12
0.54 (B)	4.04	2.88	7.05	75	239	0.11
0.54 (B) plateau[d]	4.04	2.90	7.10	87	280	0.13
0.48	4.06	2.88	7.05	99	321	0.15
0.46	4.05	2.85	6.98	91	292	0.13
0.42	4.04	2.96	7.25	115	377	0.17
0.40 no aging	4.22	3.11	7.62	76	232	0.11
0.40	4.00	3.00	7.35	127	417	0.19
0.40 (B)	3.97	3.02	7.40	123	399	0.18
0.40 (B) plateau[d]	3.97	3.04	7.45	133	432	0.19
0.40 (B) 550 °C[e]	3.97	2.90	7.10	105	337	0.15
0.27	3.90[f]	3.03[f]	7.42[f]	139	450	0.20

[a] Samples denoted B correspond to scaled-up batches. [b] The BET surface area has no reliable physical meaning for the materials described herein. It is described as BET equivalent surface area and used to compare series of samples. [c] Pore volume measured from a *t*-plot curve. The linear fit is performed with Harkins and Jura statistical thickness in the range of 0.6−1.2 nm. [d] Calcination performed with a plateau at 300 °C for 3 h, followed by a step at 500 °C for 3 h. [e] Calcination temperature. [f] No clear structural assignment possible.

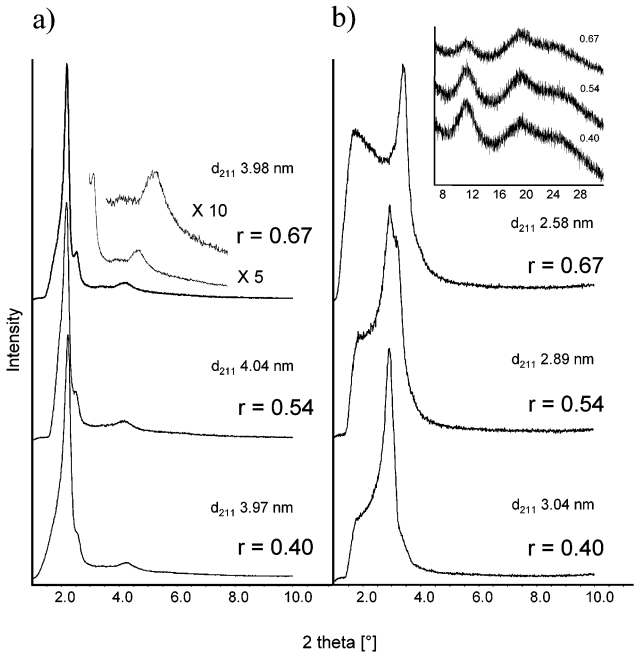

Figure 2. XRD patterns obtained on dried as-synthesized cubic zirconium oxophosphate synthesized with initial surfactant-to-zirconium sulfate ratios $r = 0.67$, 0.54, and 0.40. The samples were obtained from the scaled-up batches (B): (a) as-prepared, template-containing samples; (b) calcined samples (3 h at 300 °C and 3 h at 500 °C). The inset is the expanded region from 8 to 32° (2θ) for the same materials.

dered mesophase which may not correspond strictly to the cubic $Ia\bar{3}d$ space group. Scaling up the synthesis batch results in improved materials in terms of structure and thermal stability.

Transmission electron microscopy (TEM) has been shown recently to be a powerful tool to characterize in detail three-dimensional porous solids, and full structure solution can be achieved.[39−42] The cubic $Ia\bar{3}d$ symmetry is confirmed by HREM.

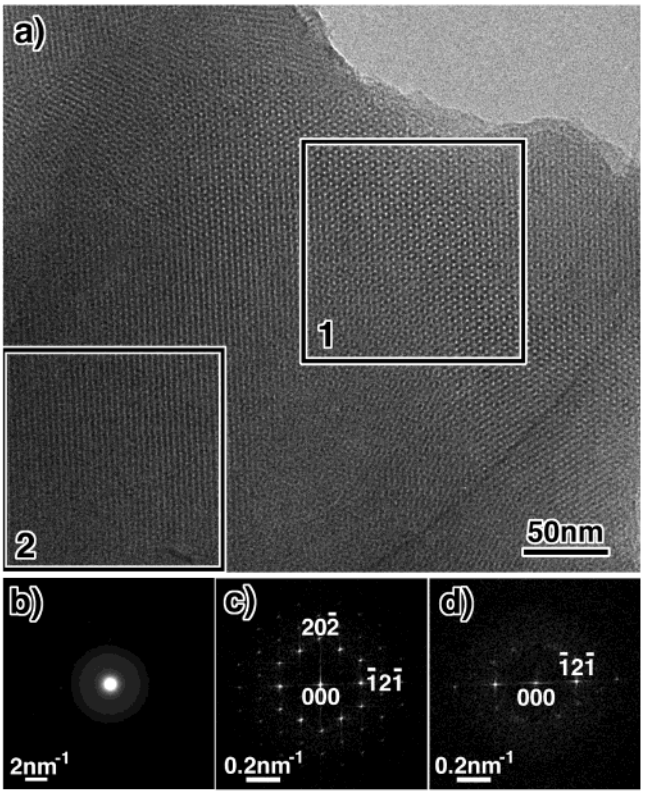

Figure 3. Typical HREM image and ED pattern of as-prepared sample B with $r = 0.54$. (a) is the HREM image taken along the [111] zone axis. (b) is the electron diffraction pattern. (c) and (d) are Fourier diffractograms obtained from the HREM images in the rectangular areas labeled by 1 and 2.

Figure 3 shows a typical HREM image and electron diffraction (ED) pattern, respectively, of an as-prepared

(39) Alfresson, V.; Anderson, M. W. *Chem. Mater.* **1996**, *8*, 1141.
(40) Schmidt, R.; Stöcker, M.; Akporiaye, D.; Tørstad, E. H.; Olsen, A. *Microporous Mater.* **1995**, *5*, 1.
(41) Carlsson, A.; Kaneda, M.; Sakamoto, Y.; Terasaki, O.; Ryoo, R.; Joo, S. H. *J. Electron Microsc.* **1999**, *48*, 795.
(42) Sakamoto, Y.; Kaneda, M.; Terasaki, O.; Zhao, D. Y.; Kim, J. M.; Stucky, G. D.; Shin, H. J.; Ryoo, R. *Nature* **2000**, *408*, 449.

sample with $r = 0.54$. Despite the relatively low resolution of the X-ray diffraction pattern, the HREM image (Figure 3a) reveals domains of highly ordered mesostructure. In the ED pattern (Figure 3b), we can observe only diffuse rings indicating that the wall structure of the as-prepared sample is amorphous; i.e., the inorganic framework is composed of amorphous zirconium oxophosphate species. Panels c and d of Figure 3, which are Fourier diffractograms obtained from the HREM images at rectangle areas labeled by 1 and 2, suggest that the material is commensurate with $Ia\bar{3}d$ symmetry. The very weak reflections of the (110) type, which are forbidden for $Ia\bar{3}d$, are not genuine, but induced by multiple-scattering effects, as the crystal contains a heavy element, Zr, and the specimen is thick. All peaks in powder XRD are indexed by this symmetry. As a whole, we can conclude that the crystal has $Ia\bar{3}d$ symmetry. The image in area 2 looks like the two-dimensional, layered type of mesoporous material. However, we can observe weak reflections in Figure 3d showing that this area corresponds to the $Ia\bar{3}d$ phase but slightly tilted off relative to the domain 1 along the $-12-1$ axis keeping the same lattice fringe of $-12-1$. It is to be noted that the length scales in reciprocal space are different for Figure 3b and Figure 3c,d, which are suitable for observing atomic-scale ordering and for mesoscale ordering, respectively.

Figure 3 indicates that the architecture of the zirconium oxophosphate surfactant mesophase synthesized in the presence of *N*-benzyl-*N*,*N*-dimethyloctadecylammonium ions is characteristic of the cubic $Ia\bar{3}d$ phase. Furthermore, the other as-prepared samples synthesized with different surfactant-to-zirconium molar ratios show the same results.

The zirconium sulfate-based mesophase is an intermediate product, which collapses upon calcination if the phosphatation is not performed. Phosphatation leads to replacement of sulfate by phosphate. This is corroborated by the sulfur and phosphorus contents of the respective samples, which were found to be quite analogous to the hexagonal phase zirconium-based mesophases.[16,31] The S/Zr ratios (wt %) have been evaluated by EDX analysis for the zirconium-based mesophases at different stages of the synthesis. The results obtained are S/Zr = 0.29, 0.27, and 0.05, after precipitation, after treatment at 90 °C, and after phosphatation, respectively. One can note that the S/Zr decreases from about 0.27 to 0.05 upon phosphatation, which corresponds to a removal of more than 80% of the sulfur content, relative to Zr. It has not been possible to remove all the sulfate contained in the material. However, according to the EDX, a zirconium oxophosphate sample before calcination contains only ~1−1.5 wt % sulfur, with an average P/Zr = 0.45.

Removal of the Template. Previous attempts to remove the template from the zirconium oxophosphate cubic mesophase by thermal treatment failed and led to collapse of the framework. To study the dramatic effects of the calcination on the inorganic−surfactant composite, we performed thermogravimetry/differential thermal analysis (TG-DTA) in combination with mass spectrometry at different synthesis stages. We showed in a previous study[35] that the TG-DTA/MS is suitable to investigate chemical and physical aspects of the template degradation and give insight in the composition of the mesophase. In addition, high-temperature XRD measurements were carried out to follow the evolution of the structure during the temperature program.

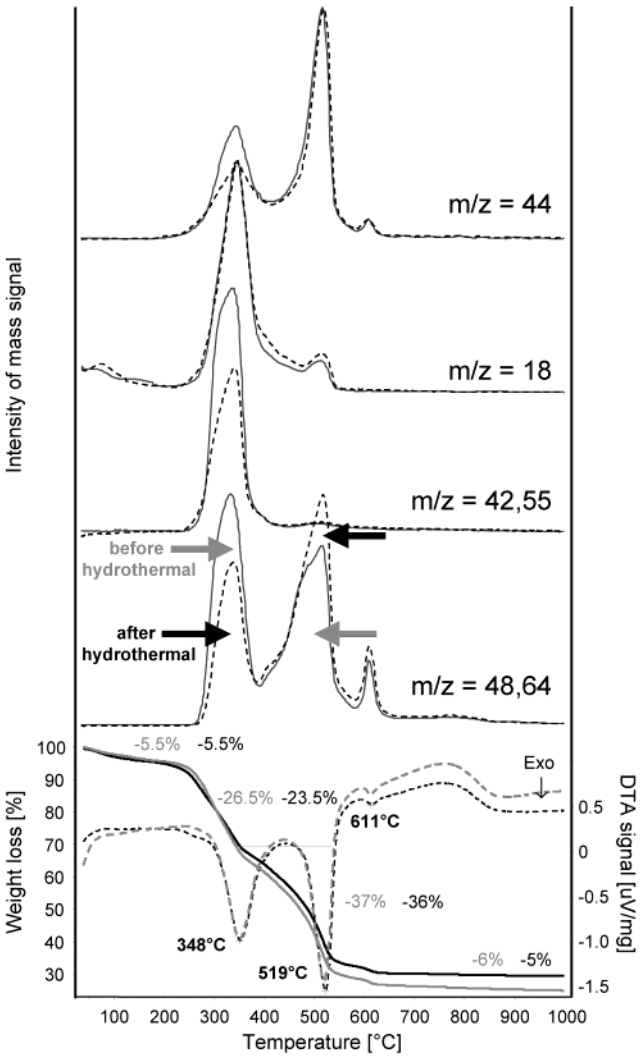

Figure 4. TG-DTA/MS measurements performed on a zirconium sulfate cubic mesophase with $r = 0.54$ before phosphatation (5 °C/min under air). The TGA data are presented at the bottom with a solid line and the DTA curve with a dashed line. The gray lines correspond to a measurement carried out on a sample prior to hydrothermal treatment. Above these are plotted various molecular species detected in the MS measurement and their evolution with temperature. Solid lines correspond to fragments obtained for a sample before hydrothermal treatment. Dashed lines correspond to fragments measured on a sample hydrothermally aged. The gray and black arrows indicate intensity variations for the peaks observed in the SO_2 traces (m/z = 48 and 64) before and after hydrothermal treatment, respectively.

Figure 4 shows the TG-DTA/MS measurement performed on the cubic zirconium sulfate−surfactant mesophase with $r = 0.54$, being the standard sample. The zirconium sulfate−surfactant mesophase was shown to collapse upon thermal treatment between 250 and 300 °C, resulting in an amorphous material with no long-range order. From the TG curve, a total weight loss of 75% is measured for a sample not hydrothermally treated. After aging, the weight loss decreases to 70%. After water desorption, three major steps in the DTA

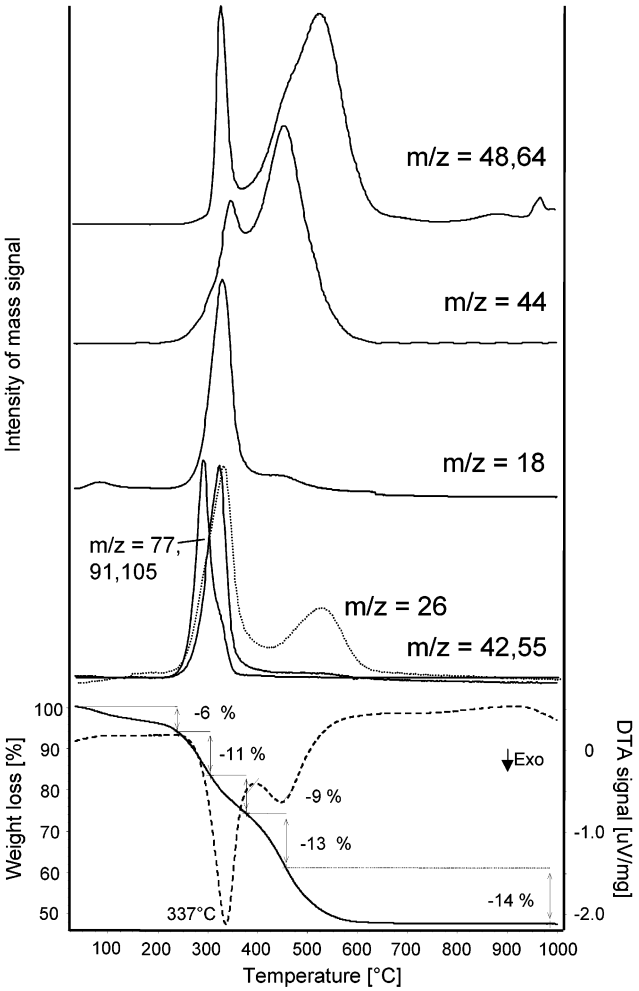

Figure 5. TG-DTA/MS measurements performed on an as-prepared zirconium oxophosphate with $r = 0.54$ (5 °C/min under air). At the bottom are shown the TGA data with a solid line and the DTA curve with a dashed line. Above these are plotted various molecular species detected in the MS measurement and their evolution with temperature.

are observed corresponding to exothermic processes. In parallel, three distinct steps are observed in the MS for the CO_2 and SO_2 traces. About 25% of the sample mass is lost in the first oxidation step, with large release of hydrocarbon, H_2O, CO_2, and SO_2. A second oxidation step, which results in a higher energy release occurs around 500 °C, where carbonaceous species, water, and SO_4^{2-} are removed (~40% in weight loss). Finally, a small step is observed at 610 °C (5%), where only CO_2 and SO_2 are detected. Samples measured after hydrothermal treatment display different TG-MS profiles. These samples exhibit a decreased relative ratio between the first mass loss step and the second, and a decrease of the first CO_2 and SO_2 peaks relative to the second ones is observed.

Figure 5 shows the TG-DTA/MS performed on the zirconium oxophosphate surfactant mesophase. The TG and DTA curves are very similar to the ones reported for hexagonal zirconium oxophosphate mesophases.[35] The total weight loss is reduced to 53% after phosphatation. Only two exothermic steps are observed. The first step corresponding to the total conversion of hydrocarbon species occurs with high energy release. The weight loss is comparable to the one observed for the nonphosphated samples (20−25%). It is followed by a second broad exothermic step with lower energy release corresponding to release of carbon dioxide and, subsequently, sulfur dioxide. Compared to the nonphosphated sample, the weight loss is reduced in this second step to ~25%. The final SO_2 step observed above 550 °C for the zirconium sulfate mesophase is not seen in the phosphated samples. Furthermore, a difference is observed in temperature for the release of the surfactant headgroup (below 300 °C), consisting of benzyldimethylammonium, compared to the carbon chain, which appears at slightly higher temperature (320 °C).

Table 2. Mass Loss Measured on the As-Prepared Dried Cubic Mesophases for Different Initial Amounts of Surfactant and Extent of Lattice Shrinkage upon Template Removal

surfactant amt:	8.59 mmol $r = 0.67$	6.87 mmol $r = 0.54$	5.15 mmol $r = 0.40$
total mass loss (%)	57	54	48
lattice shrinkage (nm)	3.43−3.48	2.90	2.27−2.45

Our experiments suggest that scaling up of the synthesis batch seems to produce materials with higher thermal stability (Table 1). The following will therefore focus on materials obtained under such conditions. Panels a and b of Figure 2 show the XRD patterns recorded for scaled-up samples synthesized with different surfactant-to-zirconium sulfate ratios before and after calcination, respectively. Increasing the initial surfactant amount resulted in a slight increase in the structural ordering. However, after calcination, a reverse tendency is observed. The structure shrinks drastically in all cases and the (220) reflection appears as a shoulder. No higher order reflections can be detected. Furthermore, the presence of a shoulder below the (211) reflection is observed. This might be due to low-angle scattering caused by small amorphous nanoparticles. This is supported by the very broad signals with low signal-to-noise ratio observed at higher 2θ angles for all calcined samples (Figure 2b inset).

The weight losses measured for the same samples with $r = 0.67$, 0.54, and 0.40 are listed in Table 2. A sample synthesized with $r = 0.67$ contains 57% organics and undergoes the largest lattice shrinkage with 3.48 nm. A lower amount of template incorporated within the mesophase results in lower shrinkage upon thermal treatment.

The sample with $r = 0.40$ seems therefore to be the more thermally stable. The result of an in situ X-ray diffraction measurement during calcination performed on this sample is shown in Figure 6a. In an attempt to reduce the strong effect of the first exothermic step occurring when the template is oxidized, the sample was calcined for 3 h at 300 °C followed by 3 h at 500 °C, since the heating ramp has a critical effect on the mesostructure. From the developing XRD patterns, a strong increase in intensity of all reflections up to 300 °C is observed, due to removal of the organics from the pores. Slight variations in intensity that accompany the template removal at higher temperature are most likely associated with modifications in structure coherency or possible thermal expansion effects. No indications of phase transformation are observed during the thermal process. The high-order reflections vanish around 450 °C. The simultaneous evolution of the $d(211)$ can be

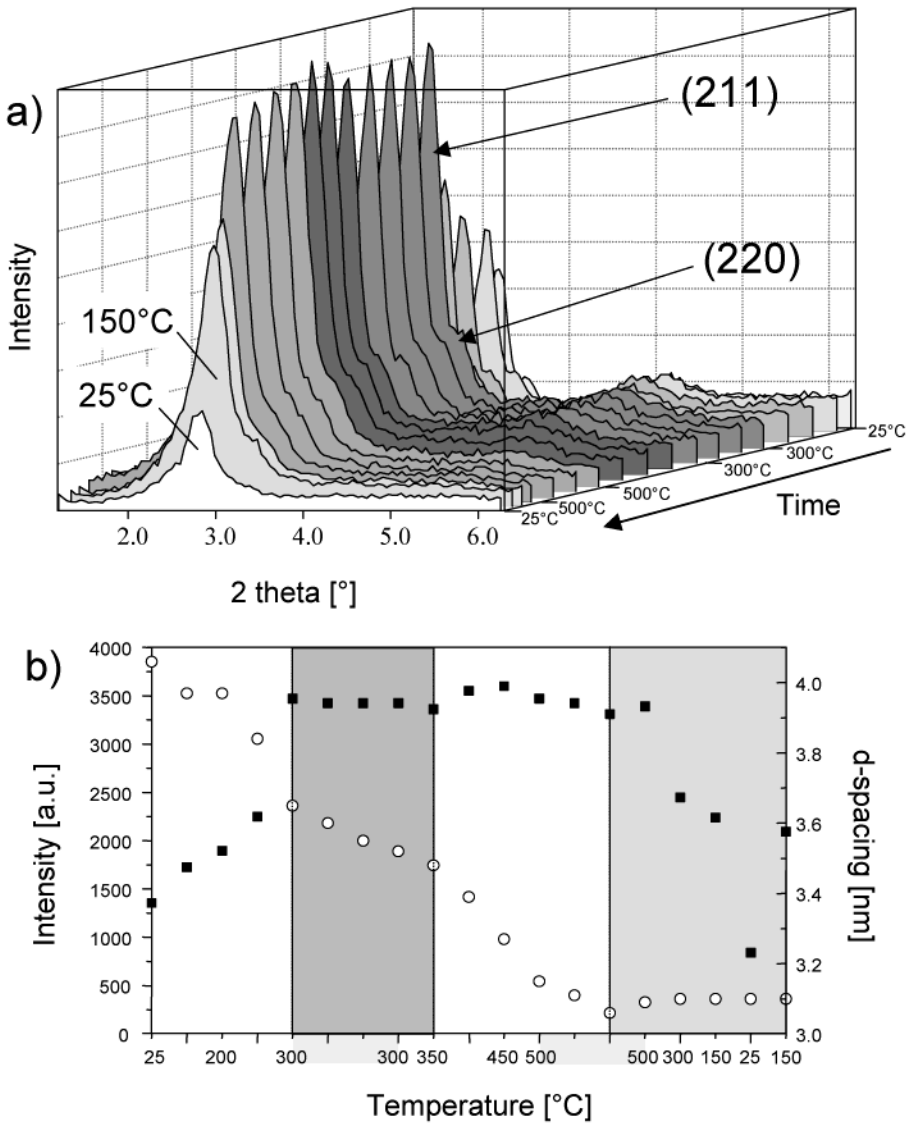

Figure 6. (a) XRD patterns stack plot obtained during in situ XRD from a cubic zirconium oxophosphate synthesized with $r = 0.40$ (heating ramp 1 °C/min). (b) Plot representing the *d* spacing and the (211) reflection intensity as a function of time and temperature (○, *d*(211) spacing; ■, intensity of the reflections).

divided into four temperature-dependent periods (Figure 6b). The *d*(211) value decreases as the calcination proceeds and remains constant during the cooling stage. Upon cooling from 150 °C to room temperature, a strong reversible decrease in the reflection intensity is observed. Calcination performed at higher temperature (550 °C) seems to diminish this effect. The reversible decrease of intensity can be attributed to the adsorption of water, as already shown for the hexagonal zirconium oxophosphate.[35] This evolution of the cubic mesophase is also representative of other samples. However, for other samples, larger *d* spacing shifts and stronger intensity variations might occur.

The elemental analysis made by EDX gives sulfur contents of less than 0.5 wt % for the calcined materials, with S/Zr < 0.02. The average P/Zr in the calcined materials remains 0.45, with average phosphorus contents of ∼13 wt %. These data are similar to the results reported for the calcined hexagonal-phase zirconium oxophosphate (0.2 wt % S; 10 wt % P), suggesting that the composition of the zirconium oxophosphate is similar to $4ZrO_2 \cdot P_2O_5$ ($+SO_4$).[31]

Structure and Properties of Porous Cubic Zirconium Oxophosphate. The samples after calcination are further characterized by TEM, XRD, and N_2 sorption. Figure 7 shows a typical HREM micrograph and ED pattern obtained for a calcined sample (B) synthesized with $r = 0.54$. Although the X-ray diffraction patterns recorded for calcined materials are poorly resolved, the HREM image (Figure 7a) reveals again domains of highly ordered mesostructure. The EM image presented is consistent with the $Ia\bar{3}d$ symmetry proposed and shows clearly the uninterrupted channels along the [111] zone axis corresponding to pores in projection. In the electron diffraction pattern (Figure 7b), one can observe diffuse electron diffraction rings, indicating that the walls remain essentially amorphous after calcination and could at most consist of very small nanoparticles. This is also supported by the absence of wide-angle reflections in the XRD pattern. Figure 7c is the Fourier diffractogram obtained from the HREM image at the labeled rectangle area. It suggests that the zirconium oxophosphate material is commensurate with the $Ia\bar{3}d$ symmetry also after calcination. Therefore,

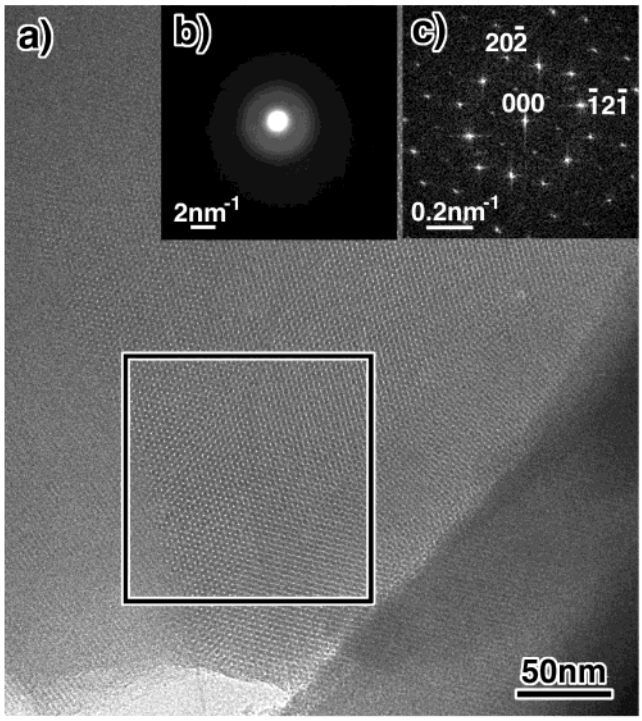

Figure 7. Typical HREM image and ED pattern of a sample (B) with $r = 0.54$ after calcination for 3 h at 300 °C and 3 h at 500 °C. (a) is the HREM image taken along the [111] zone axis. (b) is the electron diffraction pattern. (c) is the Fourier diffractogram obtained from the HREM image in the labeled rectangular area.

Figure 7 gives the evidence that the cubic $Ia\bar{3}d$ mesostructure is retained after the removal of the template by thermal treatment. Samples B with $r = 0.40$, 0.54, and 0.67 investigated by EM show similar well-resolved cubic domains.

The structural and physical properties of calcined materials synthesized with increasing surfactant-to-zirconium ratios are reported in Table 1. The XRD data of materials calcined at 500 °C give lattice parameters ranging from ~6.1−7.4 nm. When $r = 0.67$, a pronounced decrease of the d spacing down to 2.59 nm is measured, the lattice parameter being $a = 6.34$ nm. For $r = 0.40$, the $d(211)$ of the calcined sample is 3.04 nm; the resulting lattice parameter is $a = 7.45$ nm. In conclusion, one can see that decreasing the amount of surfactant results in materials having larger lattice parameter. Therefore, the amount of surfactant used seems to have a direct influence on the thermal stability of the materials. Note that the lattice parameters measured after template removal are still substantially smaller than the ones reported for conventional calcined Si-MCM-48 ($a = 8.4-10.2$ nm)[43,44] which are commonly synthesized with a C16 chain surfactant, indicating substantially smaller pore sizes. This is compatible with results for the hexagonal phase where also substantially smaller pores were found for the same surfactant, compared to MCM-41.[45] Calcination performed at 550 °C for $r = 0.40$ resulted in a larger shrinkage of the structure with $a = 7.10$ nm. Figure 8a shows N_2-

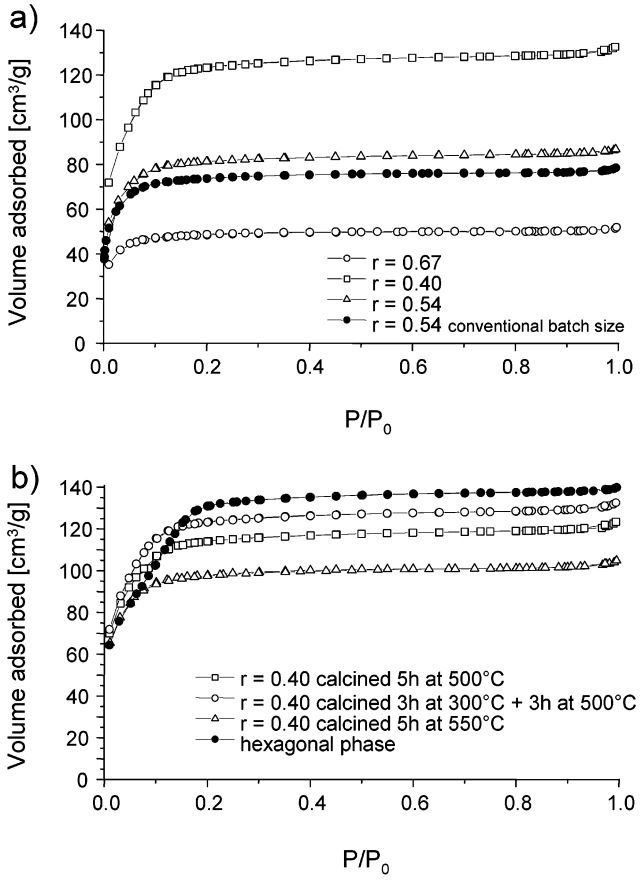

Figure 8. N_2 sorption isotherms of porous cubic zirconium oxophosphate materials obtained from scaled-up batches (B). (a) Isotherms obtained on samples with $r = 0.67$, 0.54, and 0.40. Solid symbols correspond to a sample from a conventional batch with $r = 0.54$. (b) Isotherms measured for $r = 0.40$ for different calcination programs.

sorption isotherms recorded for the samples with $r = 0.67$, 0.54, and 0.40. The isotherms are similar to type I isotherms characteristic for microporous materials. The isotherms without an obvious capillary condensation step correspond to pore sizes in the upper micropore range or lower mesopore range. We did not attempt to extract pore sizes from the isotherms, since no appropriate algorithms to calculate pore sizes are available as yet. Pore sizes calculated for silica MCM-48 with isotherms, which closely correspond to each other, deviate by more than 30%, if analyzed with different algorithms (compare, for instance, refs 46 and 47). DFT analysis is probably the most reliable technique, and it has been applied to the analysis of silica MCM-48.[47−49] However, previous analyses have been carried out for materials with larger pores and a clear capillary condensation step where the analysis is simpler. In addition, there is no interaction potential for nitrogen or argon on zirconium oxophosphate surfaces available so far, and especially for small pore diameter, the effect of

(43) Romero, A. A.; Alba, M. M.; Klinowski, J. *J. Phys. Chem. B* **1998**, *102*, 123.
(44) Kruk, M.; Jaroniec, M.; Ryoo, R.; Joo, S. H. *Chem. Mater.* **2000**, *12*, 1414.
(45) Ciesla, U.; Unger, K.; Schüth, F. In *Characterization of Porous Solids IV*; McEnaney, B., Mays, T. J., Rouquerol, J., Rodriguez-Reinoso, F., Sing, K. S. W., Unger, K. K., Eds.; The Royal Society of Chemistry: Cambridge, U.K., 1997; p 90.
(46) Thommes, M.; Köhn, R.; Fröba, M. *J. Phys. Chem. B* **2000**, *104*, 7932.
(47) Ravikovitch, P. I.; Neimark, A. V. *Langmuir* **2000**, *16*, 2419.
(48) Ravikovitch, P. I.; Neimark, A. V. *Langmuir* **2002**, *18*, 1550.
(49) Schumacher, K.; Ravikovitch, P. I.; Du Chesne, A.; Neimark, A. V.; Unger, K. K. *Langmuir* **2000**, *16*, 4648.

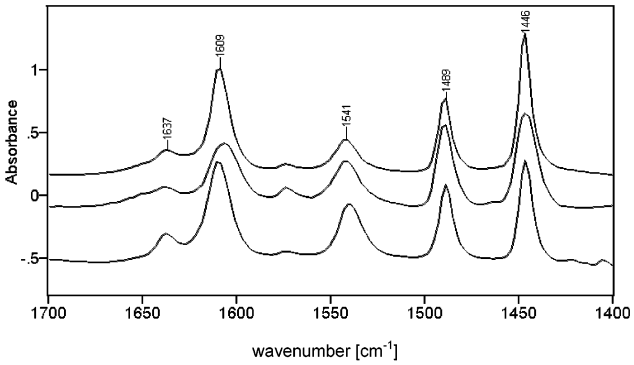

Figure 9. Spectra of three samples (B) taken at a temperature of 140 °C and a pyridine vapor pressure of 0.01 mbar: top, r = 0.40 (500 °C); middle, r = 0.40 (550 °C); bottom, r = 0.54 (500 °C). Offset is to help with clarity.

Table 3. IR Peak Assignment for Adsorbed Pyridine

H-bonded (cm^{-1})	Lewis acidity (cm^{-1})	Brønsted acidity (cm^{-1})
1400−1447	1447−1460	
	1488−1503	1485−1500
		1540
1580−1600	1580	
	1600−1633	
		1640

an inappropriate gas−solid interaction potential could have a strong influence. Instead of quoting unreliable data for pore sizes we would thus rather present the full isotherm, which can be converted to pore sizes at a later stage when better algorithms and correct potentials are available. Due to the relatively small pores, the surface area also cannot be evaluated accurately from BET calculations, and one has to be careful with the interpretation of the results. The data are given as *equivalent BET* and may only be used to underline tendencies (Table 1). The total nitrogen adsorption capacity decreases rapidly with increasing surfactant-to-zirconium sulfate ratio (see Table 1). The shape of the isotherm obtained when r = 0.40 may suggest slightly larger pores in agreement with the larger lattice parameter. In Figure 8b, isotherms obtained for different calcination programs are depicted. Also represented as a reference is a typical isotherm measured for the hexagonally ordered zirconium oxophosphate. The highest adsorption capacity is measured for the sample calcined with a plateau at 300 °C. Calcination performed at 550 °C leads to a type I isotherm with lower adsorbed volume. Finally, the cubic zirconium oxophosphate clearly shows a lower adsorption volume than its hexagonal counterpart. The step at lower relative pressure measured for the cubic material indicates clearly a smaller pore size.

Evaluation of the Acidity by Pyridine Sorption Measurements. The IR spectra of adsorbed pyridine are shown in Figure 9. The figure details spectra of three samples taken at a temperature of 140 °C and a pyridine vapor pressure of 0.01 mbar. The samples measured were two r = 0.40 samples calcined at 500 and 550 °C and one r = 0.54 sample calcined at 500 °C. The peak assignments for the pyridine adsorption spectra are detailed in Table 3.[50] In terms of relative peak intensities, the largest Brønsted/Lewis (B/L) peak ratio, determined using the ratio of the 1540- (B) and

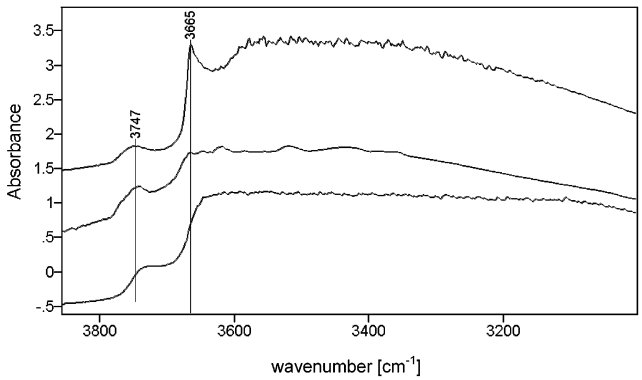

Figure 10. OH stretching region prior to pyridine adsorption: top, r = 0.40 (500 °C); middle, r = 0.40 (550 °C); bottom, r = 0.54 (500 °C). Offset is to help with clarity.

the 1446-cm^{-1} (L) peaks, was observed in the 0.54 sample. A comparison of the two r = 0.40 samples calcined at 500 and 550 °C, respectively, shows a relative increase in Brønsted acidity with increasing temperature. However, when plotted against each other on an absolute absorbance scale, the sample calcined at 550 °C showed a significant decrease in intensity of both Brønsted- and Lewis- adsorbed pyridine compared to its 500 °C counterpart. This observation is consistent with both N_2 adsorption measurements and powder XRD measurements, which proved a decrease in void volume and a loss of reflection intensity in the r = 0.40 sample at the higher calcination temperature, respectively. Both these factors, combined with the obvious decrease in the number of acid sites, show that temperatures above 500 °C result in an inferior material.

The IR spectra of the samples prior to pyridine loading (Figure 10) show the ν_{O-H} region (3000−3600 cm^{-1}) as a broad band. However, in the r = 0.40 sample, sharp and well-defined peaks were observed at 3747 and 3665 cm^{-1}. These bands are assigned to surface terminal Zr−OH groups and bridging hydroxyl species, respectively.[51] From the spectrum, it is clear that bridging hydroxyl groups are prominent in this sample but are significantly reduced upon heating to 550 °C. It follows that the synthetic conditions for producing the bridged species are reliant on the amount of surfactant used and the temperature of calcination.

Discussion

The results show that it is possible to synthesize in a simple manner a zirconium oxide-based mesoporous material that exhibits the attractive cubic $Ia\bar{3}d$ bicontinuous structure. A simple way to describe this three-dimensional structure is to consider it to be made of two continuous interconnected channel systems that are intertwined together.[39,41] The use of *N*-benzyl-*N*,*N*-dimethyloctadecylammonium chloride as the structure-directing agent in water enables the synthesis of a mesophase being structurally analogous to MCM-48.

(50) Ertl, G., Weitkamp, J., Knözinger, H., Eds. *Handbook of Heterogeneous Catalysis*; John Wiley and Sons: New York, 1997; pp 707−732.

(51) (a) Bensitel, M.; Moravek, V.; Lamotte, J.; Saur, O.; Lavalley, J.-C. *Spectrochim. Acta* **1987**, *43A*, 1487. (b) Clearfield, A.; Serrette, G. P. D.; Khazi-Syed, A. H. *Catal. Today* **1994**, *20*, 295. (c) Morterra, C.; Cerrato, G.; Bolis, V.; Di Ciero, S.; Signoretto, M. *J. Chem. Soc., Faraday Trans.* **1997**, *93*, 1179.

The zirconium sulfate mesophase is therefore also analogous to the lyotropic liquid crystal cubic $Ia\bar{3}d$ phase found in the water−CTAB system.[52]

It is possible to explain the structure of the cubic mesophase obtained by the packing parameter for micelle formation,[53] although the packing parameter concept was originally developed for dilute systems only. The formation of inorganic−organic composite mesophases is considered to be controlled by similar structural constraints observed for the usual surfactant liquid-crystal phases. Therefore, size, shape, and charge of surfactants are crucial structure-directing parameters with the packing parameter depending strongly on the volume fraction of surfactant chains.[54,55] Surfactants such as hexadecyl- or octadecyltrimethylammonium halides enable preferentially the synthesis of hexagonal mesophases. When such systems have organic additives or hydrocarbon chains located in the region between the headgroup of the surfactant and the hydrophobic core, the volume fraction of the surfactant chains increases substantially. Micellar aggregates with a slightly lower curvature result, and the cubic $Ia\bar{3}d$ structure can be favored.[56] The synthesis of the zirconium sulfate mesophase under acidic conditions using *N*-benzyl-*N*,*N*-dimethylalkylammonium chloride as template follows the same principle. The *N*-benzyl-*N*,*N*-dimethyloctadecylammonium ion might be considered as a trimethyloctadecylammonium ion with solubilized benzene molecules anchored to the ammonium headgroup. The benzene groups are located in the hydrophobic core of the micelle, leading to an increase of the effective volume of the hydrophobic tail. These packing effects together with electrostatic driving forces for self-assembly generate the bicontinuous cubic structure at low pH.

The one-pot synthesis requires then an aging period at 90 °C in order to achieve a more stable material. This procedure might increase substantially the stability of the structure. During this hydrothermal treatment, no phase change occurred as could be observed in some cases for hexagonal analogues.[37] The observed decrease of the first CO_2 and SO_2 peaks relative to the second ones in the TG-MS traces after hydrothermal treatment is probably due to the expulsion of surfactant molecules and sulfate groups from the mesophase. This may result in some decrease in ionic strength within the material, affecting the surfactant packing parameter in the organic−inorganic mesophase and the framework condensation process. However, it is not clear whether this phenomenon plays an important role in the stabilization of the cubic mesophase.

The zirconium sulfate surfactant mesophases show a large organic template content with more than 65−70% weight loss before 500 °C. The strong oxidation processes of the organic chains and the high content in thermally unstable sulfate species account for the structural collapse. A subsequent efficient posttreatment with phosphoric acid is the key step to generate a material stable upon thermal treatment. This phosphatation step occurs without phase transformations in contrast to previous reports on zirconia mesophases.[20] Nonneglible amounts of surfactant species seems to be removed from the mesophase during this phosphatation treatment. According to the TG data, the total weight loss decreases from ∼70% before phosphatation down to ∼50% for the phosphated materials (with small variations depending on the samples). Since the inorganic species are negatively charged, the interaction between surfactant molecules and inorganic is proposed to be S^+I^-. The phosphate groups replace the sulfate groups in the mesophase; however, the exact location of the phosphate groups (framework walls, surface, and interface with the surfactant) has not been clarified yet. Taking into account that sulfate groups and surfactant molecules are removed, it is likely that the sulfate groups and the alkylammonium groups form ion pairs and are, therefore, displaced from the mesophase, as $(S^+)_2SO_4^{2-}$ or $S^+HSO_4^-$. The aqueous solution of phosphoric acid provides phosphates and possible countercations (H^+), allowing a kind of extraction reaction of the surfactant. However, ion pairing with PO_4^{3-} or $H_2PO_4^-$ cannot be excluded either. Last, it has to be noted that even though the zirconium sulfate mesophase forms very rapidly, the degree of condensation is relatively low and subsequent phosphatation treatment allows further condensation[37] and possible compositional/structural changes or reorganization.

Regarding the XRD results on the different as-prepared phases, it turns out that the surfactant-to-zirconium ratio range, where the cubic $Ia\bar{3}d$ mesophase with a well-resolved diffraction pattern is obtained, is rather narrow between $r = 0.40$ and $r = 0.67$. Within this r range, it seems that increasing surfactant amount leads to sharper and better resolved reflections. Comparable observations were made previously on hexagonal zirconium oxide and niobium oxide phases.[17,21]

Removal of the template has been successfully achieved upon controlling the temperature program and using a very slow heating rate. The amount of organic material is reduced substantially during phosphatation, and the sulfate groups are partly replaced by thermally stable phosphate ones. From this, the framework is efficiently stabilized, and the exothermic effects of the template oxidation on the overall structure are possibly reduced. Moreover, reduction of the amount of template incorporated by diminishing the initial amount used or upon hydrothermal restructuring seems to enhance the rigidity of the mesostructure. Indeed, a clear relationship between the surfactant proportion and the stability of the materials upon calcination is observed. However, the *d* spacing of the as-prepared zirconium oxophosphate-surfactant mesophases is not influenced by the amount of surfactant initially added, even if the materials with lower surfactant-to-zirconium ratio contain less surfactant as shown by the TG experiments. This would indicate a larger proportion of inorganics, which points toward thicker framework walls. On the other hand, a mesophase synthesized with low surfactant amounts could also consist of less compact micellar inorganic−

(52) Auvray, X.; Petipas, C.; Anthore, R.; Rico, I.; Lattes, A. *J. Phys. Chem.* **1989**, *93*, 7458.
(53) (a) Israelachvili, J. N.; Mitchell, D. J.; Ninham, B. W. *J. Chem. Soc., Faraday Trans. 2* **1976**, *72*, 1525. (b) Israelachvili, J. N.; Mitchell, D. J.; Ninham, B. W. *Biochim. Biophys. Acta* **1977**, *470*, 185.
(54) Huo, Q.; Margolese, D. I.; Stucky, G. D. *Chem. Mater.* **1996**, *8*, 1147.
(55) Firouzi, A.; Atef, F.; Oertli, A. G.; Stucky, G. D.; Chmelka, B. F. *J. Am. Chem. Soc.* **1997**, *119*, 3596.
(56) Morey, M. S.; Davidson A.; Stucky, G. D. *J. Porous Mater.* **1998**, *5*, 195.

surfactant aggregates. The stronger deterioration of materials obtained with higher surfactant content could either result from lower thermal stability of thinner walls or from higher local heating caused by the burning of more organic substances. Furthermore, compared to a system based on a usual trimethylalkylammonium halide template,[35] the decomposition of the surfactant with the headgroup leaving at lower temperature suggests different interactions between the benzyldimethylammonium headgroup and the inorganic framework.

Shrinkage of the structure and partial loss of long-range ordering are phenomena usually observed for transition metal-based mesophases, caused by relatively low thermal stability, incomplete condensation, and redox processes occurring within the structure during calcination. Nevertheless, the porous cubic zirconium oxophosphates described in this work exhibit fairly well-ordered structures and interesting chemical and physical properties. The best results in terms of organization of the porous material and adsorption capacity were obtained with surfactant-to-zirconium sulfate ratios between $r = 0.40$ and $r = 0.54$. Beyond $r = 0.54$, the structure undergoes dramatic shrinkage or collapses, showing very low nitrogen adsorption capacities. Below $r = 0.40$, the presence of another phase cannot be excluded. The high quality of the $r = 0.40$ material corresponds to the highest concentration of bridging OH groups as found by pyridine adsorption detected by IR spectroscopy, although the sample synthesized with $r = 0.54$ has a higher B/L ratio. Whether these differences are an effect of different charge compensation or packing parameter at different concentration or are caused by higher surface energies of smaller pores is unclear as yet.

The porous zirconium oxophosphate has a cubic structure with the space group $Ia\bar{3}d$. The electron microscopy images taken show usually the uninterrupted channels along the [100] and [111] zone axis corresponding to pores in projection. No channel can be observed along the [110] zone axis; only contrast variations are seen due to changes in electron density of the walls in projection. The presence of a $p6mm$ hexagonal phase is excluded. Similarly to MCM-48, one can interpret the *bicontinuous* 3-D structure of the cubic zirconium oxophosphate to be consisting of two independent continuous channel systems. The two systems are intertwined together, following the model described for $Ia\bar{3}d$ structures.[39,56] The pores in each channel system are interconnected. Both systems of channels are generated by templating with micellar aggregates of similar size and shape. Unlike SBA-15-type materials,[57,58] mesostructured materials with $Ia\bar{3}d$-type materials do not have a bimodal pore distribution. In the present case, the pore sizes are in the lower mesopore range or upper micropore range.

Calcination performed at 300 °C for 3 h, followed by 3 h at 500 °C, seems to be the most suitable protocol for the removal of the template. At higher temperature, the structure is more damaged and shrinkage is larger. A plateau in the temperature program seems to be useful for optimal structure preservation.

The samples exhibit Brønsted as well as Lewis acid properties. The $r = 0.54$ sample has the highest B/L ratio of the samples measured by pyridine adsorption, but the $r = 0.40$ (500 °C) sample has clearly more Brønsted acidic bridging OH groups. This sample also has the highest pore volume and thermal stability and shows the least lattice shrinkage upon calcination. It is at present not clear why $r = 0.40$ induces these effects. It could, for instance, be due to optimum charge compensation at this ratio or to optimal surfactant packing.

Conclusions

By carefully controlling the synthesis conditions and the removal of the template, we succeeded in synthesizing a porous cubic zirconium oxophosphate showing a very well developed cubic $Ia\bar{3}d$ structure. Detailed investigations of the template removal could be carried out by using techniques such TG-DTA coupled with MS and high-temperature XRD. The cubic structure inferred from XRD is confirmed for the template-free materials by direct observation using HREM, which enables precise structure assignment. The porous zirconium oxophosphate described is therefore one of the first transition metal-based analogues of MCM-48-type materials. The zirconium oxophosphate exhibits total nitrogen adsorption capacity of up to 130 cm^3/g and has a pore volume of up to 0.20 cm^3/g, with pore sizes reaching the upper micropore/lower mesopore range. Pyridine sorption followed by IR spectroscopy shows that the samples contain both Brønsted and Lewis acid sites, the concentrations of which depend on the synthesis parameters.

Acknowledgment. The European Community (project HPRN-CT-99-00025) and the Japan Science and Technology Corp. (O.T. and Z.L.) are gratefully acknowledged for financial support.

CM021128D

(57) Ko, C. H.; Ryoo, R.; Kruk, M.; Antochshuk, V.; Jaroniec, M. *J. Phys. Chem. B* **2000**, *104*, 11465.

(58) Impérior-Clerc, M.; Davidson, P.; Davidson, A. *J. Am. Chem. Soc.* **2000**, *122*, 11925.